The Cryosphere Discuss., doi:10.5194/tc-2016-6, 2016
Manuscript under review for journal The Cryosphere
Published: 29 January 2016

The Cryosphere Discussions
Open Access

Surface Energy Balance Sensitivity to Meteorological Variability on Haig Glacier, Canadian Rocky Mountains

S. Ebrahimi and S. J. Marshall

Department of Geography, University of Calgary, 2500 University Drive, NW, Calgary, Alberta T2N 1N4, Canada

Correspondence to: S. Ebrahimi (samaneh.ebrahimi@ucalgary.ca)

Abstract

Energy exchanges between the atmosphere and the glacier surface control the net energy available for snow and ice melt. Meteorological and glaciological observations are not always available to measure glacier energy and mass balance directly, so models of energy balance processes are often necessary to understand glacier response to meteorological variability and climate change. This paper explores the theoretical and empirical response of a mid-latitude glacier in the Canadian Rocky Mountains to the daily and interannual variations in the meteorological parameters that govern the surface energy balance. The model's reference conditions are based on 11 years of in situ observations from an automatic weather station at an elevation of 2660 m, in the upper ablation area of Haig Glacier. We use an energy balance model to run sensitivity tests to perturbations in temperature, specific humidity, wind speed, incoming shortwave radiation, and glacier surface albedo. The variables were perturbed one at a time for the duration of the glacier melt season, May to September, for the years 2002-2012. The experiments indicate that summer melt has the strongest sensitivity to interannual variations in incoming shortwave radiation, albedo, and temperature, in that order. To explore more realistic scenarios where meteorological variables and internal feedbacks such as the surface albedo co-evolve, we use the same perturbation approach using meteorological forcing from the North American Regional Reanalysis (NARR) over the period 1979-2014. These experiments provide an estimate of historical variability in Haig Glacier surface energy balance and melt for years prior to our observational study. The methods introduced in this paper provide a methodology that can be employed in distributed energy balance modelling at regional scales. They also provide the foundation for a theoretical framework that can be adapted to compare the climatic sensitivity of glaciers in different climate regimes, e.g., polar, maritime, or tropical environments.

1. Introduction

Glaciers and icefields are thinning and retreating in all of the world's mountain regions in response to global climate change (e.g., Marzeion et al., 2014). This is reshaping alpine environments, affecting regional water resources, and contributing to global sea level rise (e.g., Radić and Hock, 2011).

Melting of glaciers in response to climate warming might be considered banal or trivial; snow and ice are threshold systems, no longer viable when temperatures rise above 0°C. Nonetheless, glaciers are perhaps more responsive to climate warming than would be expected from the many detailed surface energy balance studies that have been carried out (e.g., Arnold et al., 1996; Hock and Holmgren, 1996, 2005; Greuell and Smeets, 2001; Klok and Oerlemans, 2002; Braun and Hock, 2004). These studies indicate that shortwave radiation is the leading term in the surface energy budget, responsible for 60-90% of the available melt energy at extratropical glaciers. Air temperature modulates incoming longwave radiation and sensible heat flux, but these are generally less important terms for glacier melt.

The meteorological controls of snow and ice melt are important to understand and to portray correctly in projections of glacier sensitivity to climate change. For pragmatic reasons, regional- to global-scale models of glacier mass balance commonly employ temperature-index methods to parameterize glacier melt (e.g., Hock, 2005; Marzeion et al., 2014; Clarke et al., 2015). This is a reasonable approach, in that the distributed meteorological fields needed for a complete surface energy balance are not well-modelled in mountain regions. This is particularly true at global scales and in future projections, where climate reanalysis are not available to drive detailed regional climate models.

While temperature-index methods have been shown to do a reasonable job at capturing seasonal melt (Hock, 2005), they are nonetheless missing much of the physics that govern snow and ice melt. Moreover, they require local calibration for degree-day melt factors and therefore are not clearly portable in space and time. The choice of single values for melt factors for snow and ice broadly captures the effects of different albedo values for these two surfaces, but it does not allow for the continuous and systematic progression of surface albedo change that is observed on glaciers during the melt season (e.g., Brock et al., 2000; Cuffey and Paterson, 2010).

Because temperature-index models estimate snow and ice melt as a function of air temperature, these models may also be overly sensitive to changes in temperature, and will not effectively capture the impact of shifts in, e.g., wind, humidity, cloud cover, surface albedo, or incoming shortwave radiation. Energy balance processes also differ between glacierized regions, such that their sensitivity to variations in temperature will not be uniform. For example, latent heat flux is crucial to tropical glaciers (e.g., Wagnon et al., 1999, 2003; Favier et al., 2004), such that perturbations to humidity and wind might be expected to matter more here, relative to a change in temperature.

Several studies have examined the sensitivity of glacier mass balance to variations in temperature and precipitation (e.g., Oerlemans, 1992; Oerlemans and Fortuin, 1992; Braithwaite et al., 2002; de Woul and Hock, 2005; Anderson et al., 2010), but studies examining the full surface energy balance are limited. Denby et al. (2002) examined the sensitivity of glacier energy balance to variations in climate on the Greenland Ice Sheet. Following up on this idea, we introduce a sensitivity-analysis approach to examine changes in the surface energy and mass balance of Haig

The Cryosphere Discuss., doi:10.5194/tc-2016-6, 2016
Manuscript under review for journal The Cryosphere
Published: 29 January 2016

The Cryosphere Discussions

Glacier in the Canadian Rocky Mountains in response to daily and interannual variations in meteorological conditions. Haig Glacier is the main outlet of a small icefield (3.3 km^2) that straddles the North American continental divide, flowing southeastwards and spanning an elevation from 2425-2950 m. Direct observations of meteorological conditions and surface energy and mass balance are available from Haig Glacier since 2002 (Marshall, 2014). The melt season runs from May to September (MJJAS) at this site, with more than 80% of the melt occurring in the summer months of June through August (JJA).

We report the mean monthly melt season (MJJAS) meteorological and energy balance conditions on the glacier for the period 2002-2012, based on automatic weather station (AWS) records. These reference data are then used as a baseline for sensitivity tests that assess the impact of changes in different meteorological parameters on summer melt extent. The same perturbation approach is then used to reconstruct variations in surface energy balance and melt for the period 1979-2014, based on North American regional climate reanalysis (NARR) (Mesinger et al., 2006).

2. Background

The energy budget at the glacier surface is defined by the fluxes of energy between the atmosphere, the snow/ice surface, and the underlying snow or ice. The surface energy balance can be written

$$Q_N = Q_S^{\downarrow}(1-\alpha) + Q_L^{\downarrow} - Q_L^{\uparrow} + Q_H + Q_E + Q_C, \qquad (1)$$

where Q_N is the net energy flux at the surface and $Q_S^{\downarrow}$, $Q_L^{\downarrow}$, $Q_L^{\uparrow}$, Q_H, Q_E, and Q_C represent incoming shortwave radiation, incoming and outgoing longwave radiation, sensible and latent heat flux, and subsurface conductive energy flux, respectively. The surface albedo is denoted α and fluxes are defined to be positive when they are sources of energy to the glacier surface. This expression of the surface energy balance neglects the penetration of shortwave radiation and advection of energy by precipitation and meltwater fluxes.

On a melting glacier surface ($Ts = 0$°C) with $Q_N > 0$, the net energy flux is dedicated to generating surface melt, with melt rate $\dot{m}$, following

$$\dot{m} = \frac{Q_N}{\rho_w L_f}, \qquad (2)$$

where ρ_w is the density of water and L_f is the latent heat of fusion. Melt rates in (2) have unit m water equivalent per second (m w.e. s^{-1}).

Numerous studies have shown that incoming shortwave radiation is the dominant term in the energy balance during the melt season in most glacial environments. Incoming shortwave radiation (insolation) at the surface has two main components: direct and diffuse solar radiation. A third contribution, direct light that is reflected from the surrounding terrain, can also add to the surface insolation. Direct solar radiation is the radiative flux from the direct solar beam, which comes in at a zenith angle Z, and is a function of latitude, time of year, and time of day (e.g., Oke, 1987). Potential direct (clear-sky) incoming solar radiation on a horizontal surface can be estimated from

The Cryosphere Discuss., doi:10.5194/tc-2016-6, 2016
Manuscript under review for journal The Cryosphere
Published: 29 January 2016

The Cryosphere Discussions

$$Q_\phi^{\downarrow} = Q_0 \cos(Z)\, \varphi_0^{P/P_0 \cos(Z)}, \tag{3}$$

for top-of-atmosphere insolation Q_0, clear-sky atmospheric transmissivity ψ_0, air pressure P, and sea-level air pressure P_0 (Oke, 1987). Eq. (3) allows potential direct shortwave radiation to be calculated at a site as a function of the day, year, latitude and elevation.

Longwave radiation can be estimated from the Stefan-Boltzmann equation,

$$Q_L = \varepsilon \sigma T^4, \tag{4}$$

where ε is the thermal emissivity, σ is the Stefan--Boltzmann constant, and T is the absolute temperature of the emitting surface. Snow and ice emit as near-perfect blackbodies at infrared wavelengths, with surface emissivity $\varepsilon_s = 0.98$-1.0. To good approximation then,

$$Q_L^{\uparrow} = \sigma T_s^4, \tag{5}$$

and

$$Q_L^{\downarrow} = \varepsilon_a \sigma T_a^4, \tag{6}$$

for surface temperature T_s, near-surface air temperature T_a, and atmospheric emissivity ε_a. Terrain emissions (i.e. from the surrounding topography) can also contribute to the incoming longwave radiation, particularly at sites that are adjacent to valley walls.

A spectrally- and vertically-integrated radiative transfer calculation is needed to predict the incoming longwave radiation from the atmosphere, as this depends on lower-troposphere water vapour, cloud, and temperature profiles. Because the requisite atmospheric data are rarely available in glacial environments, $Q_L^{\downarrow}$ is commonly parameterized at a site as a function of local (2-m) temperature and humidity. Where available, cloud cover or a proxy for cloud conditions, such as the atmospheric clearness index, are often used to strengthen this parameterization. Hock (2005) provides a review of some of the parameterizations of atmospheric emissivity that have been employed in glaciology. At our study sites in the Canadian Rocky Mountains, Haig and Kwadacha Glaciers, good results were found for regression-based parameterizations of the form

$$Q_L^{\downarrow} = (a + b e_v + ch)\, \sigma T_a^4 \tag{7}$$

or

$$Q_L^{\downarrow} = (a + b e_v + c\tau)\, \sigma T_a^4, \tag{8}$$

for regression parameters a, b, and c (different in Eqs. (7) and (8)), vapour pressure e_v, relative humidity h, and clearness index τ, calculated from the ratio of measured to potential direct incoming shortwave radiation.

Solar radiation and cloud data are less commonly available than relative humidity, so Eq. (7) is a slightly less accurate but more portable version of this parameterization (Ebrahimi and Marshall, in press). Multiple regressions of ε_a containing both relative humidity and clearness index were rejected, as these are highly (negatively) correlated. All-sky longwave parameterizations using

The Cryosphere Discuss., doi:10.5194/tc-2016-6, 2016
Manuscript under review for journal The Cryosphere
Published: 29 January 2016

either of these variables are reasonable, with root-mean square errors in mean daily incoming longwave radiation of about 10 W/m^2.

Relative humidity can also be used as a reasonable proxy of clearness index if shortwave radiation data are not available. Observations at Haig Glacier follow the relation:

$$\tau = 1.3 - 0.01h\ , \tag{9}$$

for mean daily values of τ and h. We draw on this below when we need to estimate perturbations in sky clearness index that are consistent with changes in atmospheric humidity.

Turbulent fluxes of sensible and latent energy in the glacier boundary layer are commonly parameterized from an eddy-diffusivity model of turbulent exchange (e.g., Andreas, 2002), also known as the profile method:

$$Q_H = \rho_a c_p k^2 v \left[\frac{T_a(z) - T_s}{\ln(^z/_{z_0})\ln(^z/_{z_{0H}})}\right], \tag{10}$$

and

$$Q_E = \rho_a L_v k^2 v \left[\frac{q_a(z) - q_s}{\ln(^z/_{z_0})\ln(^z/_{z_{0E}})}\right]. \tag{11}$$

Here ρ_a is the air density, c_p is the specific heat capacity of air, L_v is the latent heat of evaporation, k = 0.4 is von Karman's constant, v is wind speed, q refers to the specific humidity, and measurements of temperature and humidity are assumed to be at two levels, height z (e.g., 2 m) and at the surface-air interface, s. For a melting glacier surface, T_s = 0°C, and q_s can be taken from the saturation specific humidity over ice at temperature T_s. We use measurements of outgoing longwave radiation to estimate T_s, from an inversion of Eq. (5).

Parameters z_0, z_{0H}, and z_{0E} refer to the roughness length scales for turbulent exchange of momentum, heat, and moisture. Atmospheric stability adjustments can also be introduced in Eqs. (10) and (11) to modify the turbulent flux parameterizations for the stable glacier boundary layer (e.g., Hock and Holmgren, 2005; Giesen et al., 2008). In this study we do not apply stability corrections. Marshall (2014) was able to attain closure in modelled and measured summer melt at this site without including stability corrections, and others have argued that stability corrections may lead to an underestimation of the turbulent fluxes on mountain glaciers (e.g. Hock and Holmgren, 2005). This may be related to the low-level wind speed maximum that is typical of the glacier boundary layer, which introduces strong turbulence and is not consistent with the logarithmic profile of wind speed that is implicit in Eqs. (10) and (11). It may also be that the effects of atmospheric stability are absorbed in the roughness values – roughness values that are adopted to attain closure in the surface energy balance and melt calculations may be too low, masking the influences of the stable boundary layer.

Numerous short-term energy balance studies have been carried out in glacial environments. Willis et al. (2002) and Hock (2005) provide tabulations of energy balance terms reported for a number of alpine glaciers during the melt season. Distributed energy balance models based on these equations have been developed and applied to numerous glaciers (e.g., Arnold et al., 1996; Klok and Oerlemans, 2002; Hock and Holmgren, 2005; Marshall, 2014). The energy supply to mid-latitude glaciers is primarily derived from the net shortwave radiation, $Q_S^{\downarrow}(1-\alpha)$, with important contributions from $Q_L^{\downarrow}$ and Q_H. Outgoing longwave radiation, $Q_L^{\uparrow}$, is the main energy sink. Q_E and *v*aries in sign but generally acts as a small energy sink on mid-latitude glaciers, with several W m^{-2} of evaporative cooling.

Mean surface energy balance conditions measured at Haig Glacier are typical of these mid-latitude mountain glacier sites, and are summarized in the next section. These values are updated from Marshall (2014).

3. Field Site and Observational Data

Reference meteorological conditions and surface energy balance fluxes are based on *in situ* measurements at Haig Glacier in the Canadian Rocky Mountains for the period 2002-2012 (Marshall, 2014). These reference observations, along with glacier mass balance studies and ultrasonic depth gauge (SR50) data, provide an 11-year record of observed summer melt from an automatic weather station (AWS) located near the median elevation of the glacier, 2660 m (Fig. 1). This is the upper ablation area of the glacier, which generally undergoes a transition from seasonal snow to exposed glacier ice in late July or early August.

Table 1 summarizes the mean observed meteorological and conditions at Haig Glacier over this reference period. These data are gap-filled from a weather station that has operated continuously in the glacier forefield since 2001, at an elevation of 2325 m. Observational data is used to adjust for the altitudinal and environmental differences between the sites, though either a monthly offset (e.g., $T_G = T_{FF} - \Delta T$), or a scaling factor β (e.g., $v_G = \beta_v v_{FF}$). Here, subscripts $_G$ and $_{FF}$ refer to the glacier and forefield AWS sites. The temperature offset approach is equivalent to a lapse rate, or can be expressed that way for distributed modelling over the glacier. In this study we consider only the point energy balance at the glacier AWS site.

The forefield AWS has more complete data coverage than the glacier AWS. Where both stations are missing data, gap-filling is done through assignment of mean daily observational data, in order to give 100% coverage. We run our surface energy balance model at daily time steps and include a parameterized diurnal cycle in temperature and shortwave radiation in order to better capture the effects of overnight refreezing and the fraction of the day that experiences melt (Q_N and $T_a > 0$). Smaller time steps, e.g. hourly, would be less efficient and would also pose a limitation in applying this approach with reanalysis output or climate models. Longer time steps, e.g. monthly, on the other hand, would miss capturing the daily weather conditions and variability in melt.

Table 2 summarizes the monthly surface energy balance fluxes at the AWS site on Haig Glacier over the melt season, May through September. Similar to other mid-latitude sites, when averaged over the summer, incoming shortwave radiation accounts for almost 90% of the energy that is available for melt, with sensible heat flux accounting for the other 10%. Net energy peaks in August, coincident with the low-albedo glacier ice that becomes exposed at the AWS site in late July or August. About 65% of the annual glacier melt occurs in the months of July and August.

The Cryosphere Discuss., doi:10.5194/tc-2016-6, 2016
Manuscript under review for journal The Cryosphere
Published: 29 January 2016

The Cryosphere Discussions

The meteorological variables in Tables 1 and 2 can be perturbed one at a time or in combination to examine the impact on modelled summer melt at the AWS site. We do this for the historical record (2002-2012) and also for the 35-year period 1979-2014, based on meteorological reconstructions from the North American Regional Reanalysis (NARR; Mesinger et al., 2006). The latter provides a more complete picture of interannual variability. Comparison of NARR predictions with measurements over the period 2002-2012 also allows us to assess the skill with which fluctuations in surface energy balance and summer melt can be captured in an atmospheric model that does not explicitly resolve the alpine and glacier conditions.

4. Theoretical Sensitivity of the Surface Energy Balance

Surface energy balance processes and summer melt rates depend on various meteorological influences in Eqs. (3-10). Warm summers drive high melt rates and promote negative mass balance, but there are sensitivities to a wide range of weather conditions. We examine these sensitivities for atmospheric conditions that are typical of the summer melt season on mid-latitude glaciers. For quantitative illustration, we adopt the average June to August (JJA) meteorological conditions from 2002-2012 at Haig Glacier in the Canadian Rocky Mountains (Tables 1 and 2): $T_a = 5.1°C$, $h = 67\%$, $e_v = 5.7$ mb, $q_v = 4.8$ g/kg, $P = 750$ hPa, $v = 2.6$ m/s, $Q_S^{\downarrow} = 226$ W/m^2, $Q_\phi^{\downarrow} = 359$ W/m^2, $\tau = 0.63$, $\alpha = 0.55$, and $Q_L^{\downarrow} = 280$ W/m^2.

The average JJA melt at the Haig Glacier AWS site from 2002-2012 was 2480 mm w.e. We consider the main summer months here because more than 80% of the annual melt occurs in this season, and systematic changes in meteorological forcing over this period will have the highest impact on glacier melt. Weather conditions also matter in the shoulder months, May and September, but anomalies in these months have less impact on glacier melt and mass balance. We repeat the sensitivity analysis for MJJAS conditions, and present an abridged version of these results. Melt model experiments in the next section do consider the energy balance from May through September, in order to capture the complete melt season.

Sensitivity to Temperature

Air temperature appears directly in the expressions for $Q_L^{\downarrow}$ and Q_H. Temperature change may also influence the surface energy balance through influences on other variables, such as atmospheric moisture. There is no direct impact of an air temperature perturbation on $Q_L^{\uparrow}$ or Q_C for a melting glacier surface, where $T_s = 0°C$. To illustrate the form and magnitude of a response to a temperature, we differentiate each energy balance flux with respect to temperature. For incoming longwave radiation, Eq. (6), the resulting temperature sensitivity is:

$$\frac{\partial Q_L^{\downarrow}}{\partial T} = 4\sigma\varepsilon_a T_a^3 + \sigma T_a^4 \frac{\partial \varepsilon_a}{\partial T} . \qquad (12)$$

This general form applies to a range of formulations for ε_a, such as those of Brutsaert (1975), Lhomme et al. (2007), or Sedlar and Hock (2009). Adopting the parameterization in Eq. (7), which performs well at Haig Glacier,

$$\frac{\partial Q_L^{\downarrow}}{\partial T} = 4\sigma\varepsilon_a T_a^3 + \sigma T_a^4 \left(b \frac{\partial e_v}{\partial T} + c \frac{\partial h}{\partial T} \right) . \qquad (13)$$

The Cryosphere Discuss., doi:10.5194/tc-2016-6, 2016
Manuscript under review for journal The Cryosphere
Published: 29 January 2016

The last two terms reflect potential feedbacks of temperature change on humidity. While we are only considering perturbations to temperature in this section, vapour pressure and relative humidity cannot both remain constant under a temperature change. We first assume that relative humidity h remains constant, under which conditions it is also reasonable to assumed that cloud cover and sky clearness will be unchanged (e.g., Eq. 9). For constant h, e_v scales with temperature following the Clausius-Clapeyon relation for saturation vapour pressure,

$$\frac{\partial e_v}{\partial T} = \frac{h}{100}\frac{\partial e_s}{\partial T} = \frac{h}{100}\left(\frac{L_v e_s}{R_v T_a^2}\right) = \frac{L_v e_v}{R_v T_a^2}, \tag{14}$$

where $R_v = 461.5$ J kg^{-1} °C^{-1} is the gas law constant for water vapour.

For the mean JJA meteorological conditions at Haig Glacier, Eqs. (13) and (14) give $\partial Q_L^{\downarrow}/\partial T = 4.4$ W m^{-2} °C^{-1}. Temperature increases affect $Q_L^{\downarrow}$ through both the direct effect of higher emission temperatures and the indirect effect of higher atmospheric emissivity, with these two terms in Eq. (12) contributing 4.1 and 0.3 W m^{-2} °C^{-1}, respectively.

The temperature sensitivity of sensible and latent heat fluxes follow

$$\frac{\partial Q_H}{\partial T} = \frac{\rho_a c_p k^2 v}{\ln(^z/_{z_0})\ln(^z/_{z_{0H}})}, \tag{15}$$

and

$$\frac{\partial Q_E}{\partial T} = \frac{\rho_a L_p k^2 v}{\ln(^z/_{z_0})\ln(^z/_{z_{0E}})}\left(\frac{\partial q_v}{\partial T}\right), \tag{16}$$

where

$$\frac{\partial q_v}{\partial T} \approx \frac{R_d}{P R_v}\left(\frac{\partial e_v}{\partial T}\right), \tag{17}$$

for the dry-gas law constant $R_d = 289$ J kg^{-1} °C^{-1} and air pressure P, under the assumption that air pressure is independent of temperature. Table 3 gives the turbulent flux sensitivities, substituting in the mean JJA Haig Glacier meteorological conditions for roughness values z_0=1 mm and $z_{0H} = z_{0E} = z_0/100$ (Marshall, 2014). Perturbations to both Q_H and Q_E are positive with an increase in temperature and the assumption of constant h. In combination with the increase in $Q_L^{\downarrow}$, net energy over the summer months is augmented by 12 W/m^2 for a 1°C increase in temperature.

Energy balance perturbations can be related to melt rates through their combined influence on Q_N, with $\delta m = \delta Q_N / \rho_w L_f$. Table 3 summarizes these impacts on summer melt, assuming a JJA melt season. The 1°C temperature increase ($\delta Q_N = 12$ W/m^2) is equivalent to 290 mm of meltwater, if melting conditions prevail and this energy can all be directed to snow/ice melt. This is a 12% increase over the reference levels of JJA melt, 2490 mm. These are the direct impacts of higher temperatures, not accounting for potential feedbacks or non-linearity in the seasonal evolution of melt conditions.

This scenario implicitly assumes that the warmer atmosphere contains more moisture. It is not necessarily the case, particularly in the summer months at the site where higher temperatures are associated with ridging and subsidence, i.e. hot, dry conditions. If we assume that e_v is invariant with temperature, then relative humidity must change to be consistent with the temperature perturbation. Increases in temperature are associated with reduced relative humidity; an increase of 1°C with no change in e_v corresponds to a decrease of 4.3% in mean summer h at our site, to 63%. This lowers the atmospheric emissivity in Eq. (7) and impacts $\partial\varepsilon_a/\partial T$ in Eq. (13). If there is no compensating change in cloud cover, the result is a decrease in $Q_L^{\downarrow}$ which compensates the increase in sensible heat flux, resulting in a small decrease in summer melt energy.

This treatment is still not internally consistent, however. Reduced h would also be associated with decreased cloud cover. For the 1°C temperature increase, the 4% decrease in relative humidity corresponds to an increase in clearness index of 0.04 (Eq. 9), from 0.63 to 0.67. The resulting increase in shortwave radiation compensates for the decline in $Q_L^{\downarrow}$ and the net energy increases by 6.5 W/m^2, equivalent to 155 mm of JJA melt. Results are given in Table 3 for scenarios with and without associated changes in cloud cover/sky clearness.

Sensitivity to Humidity and Wind

Similar derivatives and energy balance sensitivities can be derived with respect to the other meteorological variables, to explore the sensitivity of summer melt to different weather conditions. The sensitivity of sensible and latent heat fluxes to wind perturbations follow:

$$\frac{\partial Q_H}{\partial v} = \frac{\rho_a c_p k^2 (T_a - T_s)}{\ln(z/z_0)\ln(z/z_{0H})} \ , \tag{18}$$

and

$$\frac{\partial Q_E}{\partial v} = \frac{\rho_a L_p k^2 (q_v - q_s)}{\ln(z/z_0)\ln(z/z_{0E})} \ , \tag{19}$$

while the sensitivity to humidity is:

$$\frac{\partial Q_E}{\partial q_v} = \frac{\rho_a L_p k^2 v}{\ln(z/z_0)\ln(z/z_{0E})} \ . \tag{20}$$

Incoming longwave radiation is also affected by perturbations in humidity, following:

$$\frac{\partial Q_L^{\downarrow}}{\partial q_v} = \sigma T_a^4 \frac{\partial \varepsilon_a}{\partial q_v} = \sigma T_a^4 \left(b \frac{\partial e_v}{\partial q_v} + c \frac{\partial h}{\partial q_v} \right) . \tag{21}$$

Table 3 summaries the theoretical sensitivities for specific humidity and wind perturbations of 1 g kg^{-1} and 1 m s^{-1}, respectively, assuming that temperature is unchanged. For the humidity, we present two scenarios, the first with perturbations to only the specific and relative humidity, and the second including the expected effects of an increase in relative humidity on cloud cover.

The response to a change in humidity is strong; it impacts both the latent heat flux and incoming longwave radiation, with strong effects on the latter as estimated by our parameterization of ε_a in Eq. 7. For $\delta q_v = 1$ g kg^{-1}, Q_E and $Q_L^{\downarrow}$ increase by 10.5 and 29 W m^{-2}, respectively. If maintained over the full summer, this translates to a 38% (943 mm) increase in melt. This appears to be stronger than the sensitivity to a temperature increase, but an increase in humidity of 1 g kg^{-1} is equal to 3.3 standard deviations, relative to the typical summer variability (Table 1). In contrast, summer temperature has a standard deviation of 0.8°C, so the 1°C temperature increase in Table 3 is a weaker perturbation.

Cloud feedbacks to increased humidity can also weaken the effects of the humidity perturbation. If there is no change in temperature, relative humidity increases by 14% with $\delta q_v = 1$ g kg^{-1}; following Eq. (9), this equates to a decrease in atmospheric transmissivity of 0.12, which strongly attenuates incoming shortwave radiation. This reduces the radiative and net energy by 19 W m^{-2}.

Wind perturbations have straightforward linear effects on Q_H and Q_E, with a theoretical sensitivity of +7 W m^{-2} for an increase in summer winds of 1 m s^{-1}. Sensible heat flux increases and evaporative cooling decreases slightly. A sustained wind anomaly of 1 m s^{-1} is again quite strong, relative to a standard deviation of 0.2 m s^{-1} in mean summer winds recorded at the site from 2002-2013. Over a summer melt season, it can be concluded that energy balance and melt anomalies are relatively insensitive to variations in wind speed. This is not true on short timescales, where windy periods strongly affect the turbulent heat fluxes.

Sensitivity to Net Shortwave Radiation

Net shortwave radiation is not directly dependent on air temperature, but is affected by variations in incoming shortwave radiation (e.g., due to solar variability and cloud cover) and to changes in surface albedo:

$$\frac{\partial Q_{Snet}}{\partial Q_{S0}} = (1-\alpha_S)\cos(Z)\,\varphi_0^{\,P/P_0\cos(Z)} \tag{22}$$

and

$$\frac{\partial Q_{Snet}}{\partial \alpha_s} = -Q_{S0}\cos(Z)\,\varphi_0^{\,P/P_0\cos(Z)} \quad . \tag{23}$$

The insolation perturbation shown in Table 3, $\delta Q_S^{\downarrow} = 0.6$ W m^{-2}, corresponds to a 1 W m^{-2} anomaly in the top-of-atmosphere insolation, Q_{S0}. This is reduced to 0.6 W m^{-2} as a result of the mean sky clearness index of 0.63, and the net radiation impact is further reduced to 0.3 W m^{-2} by the surface albedo.

This is consistent with a direct estimate of sensitivity to variations in solar output through Eq. (22). For summer solstice at Haig Glacier (50.7°N, 2660 m altitude) and for $\varphi_0 = 0.84$ (clear-sky conditions), $\partial Q_{Snet} / \partial Q_{S0}$ in Eq. (22) can be integrated over the daily solar path. For a 1 W m^{-2} change in top-of-atmosphere radiation, Q_{S0}, this gives a daily mean net shortwave perturbation of 0.25 W m^{-2} at the surface. Even with clear-sky conditions, only 25% of the solar perturbation is felt at the glacier surface. The net impact of daily and interannual solar variability (e.g., sunspot cycles) is therefore small. Energy balance is more sensitive to cloud cover, as captured through the sky clearness index, τ, although this is also muted by the surface albedo. An increase in τ of 0.05, from 0.63 to 0.68, translates to an increase in net energy of 8 W m^{-2} and a 5% increase in summer melt.

In contrast, the sensitivity to albedo changes is high. An increase in albedo of 0.1 creates a peak energy balance perturbation of more than 100 W m^{-2} at local noon in mid-summer. The magnitude of this effect varies with latitude, time of year, and atmospheric transmissivity.
Integrated over the daily solar path and over the summer, an albedo increase of 0.1 reduces net solar radiation by –23 W m^{-2}, giving a 22% decrease in total summer melt.

One cannot gauge the most important meteorological variable to surface energy and mass balance from the sensitivities to a unit change in Table 3, as some meteorological parameters are intrinsically more variable. To address this, we perturb each variable by one standard deviation (cf. Table 1) in the direction of increased melt: higher temperature, humidity, wind speed, incoming shortwave radiation, and a lower albedo. This might be representative of warm, sunny summer weather that causes high melt extent, but within the observed range of variability at Haig Glacier. The experiment assumes that weather conditions all align in a way to increase the net energy, which will not be true in general (e.g., warm summers are typically dry in the region).

Results are given in the last two line of Table 3, for both mean JJA and mean MJJAS conditions. For the main summer months, JJA, Q_N is augmented by 34 W m^{-2}, giving a 32% (808 mm) increase in summer melt. Increases in each component of the surface energy balance contribute to this, but shortwave radiation is the strongest component, accounting for about half of the elevated melt. This is due to both an increased clearness index (i.e. clear-sky conditions) and the decreased albedo. Of note, none of the surface energy fluxes are negligible in the perturbed energy budget. Applying the 1-σ perturbation to MJJAS conditions, results are almost identical, with an increase in Q_N of 33.5 W m^{-2}. The net shortwave radiation again accounts for about half of this perturbation. If this energy balance anomaly is maintained over a five-month period (and assuming melt conditions for this whole period), it equates to an additional 1320 mm of melt, a 43% increase over the mean value for the period 2002-2012.

The next two sections further explore the energy balance sensitivity at Haig Glacier within an energy balance-melt model. This model operates on daily time steps through the summer melt season, May through September, and allows an estimate of feedbacks associated with the evolution of albedo and interactions between weather variables over the melt season. It also permits us to explore more realistic scenarios where weather variables vary together in meteorologically-consistent ways (i.e. with real weather).

5. Modelled Sensitivity of the Surface Energy Balance

We use a point model of surface energy balance through the summer melt season, May 1 to September 30, based on daily time steps and a sinusoidal representation of the diurnal temperature cycle. The latter uses minimum and maximum daily temperatures (the daily temperature range), and is needed to determine the fraction of the day when temperatures are above 0°C (melt conditions). Refreezing is also calculated in the model, following Eq. (2), when air temperature drops below 0°C and net energy is negative; this assumes that liquid water is available at the glacier surface or in the near-surface snowpack.

The surface energy balance model uses the glacier AWS data along with Eqs. (1)-(11) above to estimate the daily energy balance and melt. Direct measurements of incoming and outgoing longwave radiation are used, where available, and we use the longwave parameterization of Eq. (7) if radiation data is missing. Otherwise, missing data are gap-filled from the Haig Glacier forefield AWS, as discussed in section 3.

Perturbations to the observed weather from 2002-2012 are used to repeat the sensitivity analyses of section 4, but with a realistic evolution of the summer melt season rather than the mean summer conditions. Meteorological variables are perturbed as follows: ±2°C for temperature, ±50% for specific humidity and wind, ±10 W m^2 for incoming shortwave radiation, and ±0.1 for albedo. Increments are set to give 40 realizations in each case, spanning the range of the perturbation. For example, temperature increments of 0.1°C are applied for the range −2 to 2°C. For each perturbation, the 'anomaly' is prescribed for all days in the original data and the energy balance program is rerun for the period 2002-2012.

Energy balance sensitivity to temperature and wind perturbations is primarily associated with the sensible heat flux. Impacts of the modelled temperature change on longwave radiation are largely cancelled out by the humidity feedbacks (Fig. 2a). Sensitivity to humidity changes is again relatively strong, through the combined impacts of latent and longwave fluxes (Fig. 2b). The latter accounts for about 68% of the net energy sensitivity to specific humidity. We do not include potential cloud feedbacks here. For increases in both temperature and humidity, the mean summer latent heat flux switches sign from negative to positive. It remains negative but relatively small under increases in wind speed (Fig. 2c). Shortwave radiation perturbations in Fig. 2d are independent of each other but are plotted together for convenience. The black line indicates net energy sensitivity to perturbations in incoming shortwave radiation, which are attenuated through the albedo. Albedo sensitivity over a range of ±0.1 (grey line) is relatively high, a variation of 28 W m^{-2} in the net energy.

The relations in Fig. 2 are close to linear, with the slope of the line corresponding to the energy balance sensitivity. These sensitivities are reported in Table 4, based on linear regressions for each curve in Fig. 2. The albedo sensitivity, $\partial Q_N/\partial \alpha_S$, should be interpreted as a decrease of 14.1 W m^{-2} for an increase in albedo of 0.1. In each experiment, all other meteorological variables are held constant except for those that are direct impacted by a perturbation (e.g., relative humidity changes with temperature).

These sensitivities in the surface energy balance and melt model are generally consistent with the theoretical sensitivities in Section 4, and document the ability to represent this in an energy-balance based melt model. There are advantages to the model, because it can include interaction effects between variables as well as feedbacks associated with the seasonal evolution of the glacier (e.g., surface albedo and roughness). The main difference between our theoretical and model-based sensitivities is for the specific humidity perturbations. In the model, observational data are used where available; our treatment neglects potential humidity feedbacks on the incoming longwave radiation where this data is directly observed rather than modelled. This decreases the sensitivity of $Q_L^{\downarrow}$ to q_v in Fig. 2b.

As in Section 4, it is difficult to compare the sensitivity to different meteorological conditions in the arbitrary experiments shown here, as different variables have different degrees of daily and interannual variability. Table 4 includes the response of Q_N to perturbations of +1 standard deviation for each variable, using the interannual MJJAS variability given in Table 1. Variations in incoming shortwave radiation (cloud cover), albedo, and temperature emerge as the three most important variables, in that order. This echoes the results from the theoretical sensitivity study.

These variables themselves can interact and are sometimes correlated. For example, sunny, higher-temperature conditions drive strong rates of melt and inducing positive albedo feedbacks (e.g. an earlier transition from snow to ice cover). To examine this effect quantitatively, we reran the temperature sensitivity experiment but including internally-driven albedo feedbacks, i.e. letting albedo evolve with the internally modelled snow aging and snow-to-ice transition at the AWS site. We use a locally-tuned model for snow-albedo darkening after Hirose and Marshall (2013), parameterizing snow albedo as a function of accumulated positive degree days. This captures the darkening of the snow and ice surface with increasing water content and impurity concentration through the melt season. Outgoing shortwave radiation flux is then calculated using albedo and the incoming shortwave radiation.

The results are plotted in Fig. 3, which includes a new line (in grey) depicting the net shortwave radiation response to the temperature perturbations. As expected, this is a positive feedback, which increases the temperature sensitivity to $\partial Q_N/\partial T$ = 15.6 W m^{-2} (°C)$^{-1}$. This almost doubles the response, such that a 1-σ (0.7°C) increase in temperature is associated with an additional 9.4 W m^{-2} of net energy available for melt.

6. Surface Energy Balance and Melt Reconstructions, 1979-2014

North American Regional Reanalysis (NARR) weather reconstructions from 1979 to 2014 were used to calculate the historical variation in the energy budget of Haig Glacier, based on the perturbation approach of Section 5 but varying multiple parameters at once. NARR has an effective spatial resolution of 32 km (Mesinger et al., 2006) and we extract mean daily data for Haig Glacier from the grid cell that contains the site in the NARR domain. Near-surface temperature, relative humidity, wind speed, pressure, incoming shortwave radiation and incoming longwave radiation were acquired.

The large area coverage of the NARR grid cell compared to the area of Haig glacier results in an inaccurate albedo which in turn results in an inaccurate outgoing shortwave radiation value. Similarly the NARR grid cell value of outgoing longwave radiation is not applicable to the glacier. Albedo is locally modelled, using the albedo parameterization discussed in Section 5. Because we confine our interest to the summer melt season, we assume the surface to be at the melting point, giving a constant value of 315 W m^{-2} from Eq. (5) for outgoing longwave radiation from the glacier.

The Cryosphere Discuss., doi:10.5194/tc-2016-6, 2016
Manuscript under review for journal The Cryosphere
Published: 29 January 2016

Table 5 lists mean values of NARR variables in the Haig Glacier grid cell for the reference period, MJJAS 2002-2012, along with their bias relative to the in situ observations. Fig. 4 plots the mean daily fields for this period. Some of the systematic bias is associated with differences in elevation between the Haig Glacier AWS (2660 m) and the mean NARR grid cell altitude (2216 m); this can account for much of the difference in air pressure and summer temperature, as correlations are otherwise high (Table 5). However, some variables such as the incoming shortwave radiation have a large bias that cannot be explained by elevation or by the contrasting NARR vs. in situ surface properties. The radiation bias indicates a systematic underestimation of cloud cover in the NARR modelled reconstructions for this site. Correlations between the NARR daily fields and the in situ data are high for most variables, other than wind, indicating a good representation of the seasonal cycle through the summer melt season.

The biases in the raw NARR fields are too large for reasonable modelling of the surface energy balance, even with conventional elevation corrections (e.g., temperature lapse rates). We adopt a perturbation approach to adjust the NARR fields, after the methods in Section 5. This involves taking the daily NARR anomaly for each variable, relative to the NARR values for the reference period, 2002-2012, and imposing this anomaly on the mean daily conditions for the site. The latter is based on the in situ observations over the reference period.

Figure 5 plots the time series of mean melt season (MJJAS) weather conditions from the adjusted NARR output for the period 1979-2014. In situ data from 2002-2012 is plotted for comparison. Interannual variability is reasonably well-captured by the reanalysis for the surface weather variables (Figs. 5a-d), in comparison with the in situ data. Year-to-year variability in the incoming shortwave and longwave radiation are less well-captured, and the variance in the NARR shortwave radiation is much lower than what is measured at the site. Nonetheless, seasonal correlations in Table 5 are strong for most variables, so there is reason to expect that bias-corrected NARR fields can provide reasonable inputs for modelling the surface energy balance and summer melt at this site.

Trends in the 36-year NARR output are small or insignificant relative to the interannual variability. Temperature has a positive trend of +0.009°C yr^{-1}, relative humidity increased by 0.08% yr^{-1}, wind speed decreased at a small and statistically insignificant rate of 0.0025 m/s yr^{-1}, specific humidity increased by 0.0087 g/kg yr^{-1}, incoming shortwave radiation has a trend of 0.24 W/m^2 yr^{-1}, and incoming longwave radiation has an insignificant negative trend. Of these variables, humidity has the strongest trend, equivalent to a 7% increase over the NARR period. Incoming shortwave radiation also increases significantly over the 36 years, by 8.6 W/m^2. The changes in radiation fluxes indicate a decrease in cloud cover in the NARR modelled reconstructions for this region, which is perhaps at odds with the humidity trends but leads to a general increase in melt energy.

Table 6 reports the modelled NARR surface energy fluxes and melt for each month, for JJA, and MJJAS, averaged over the period 2002-2012. We show the results for both the raw NARR inputs and with the perturbation approach, taking NARR fields as daily anomalies relative to the reference conditions. A comparison of different energy fluxes in Table 6 to the in situ data in Table 2 demonstrates the large error associated with direct application of the NARR fields, without bias correction. On the other hand, the model treatment which takes NARR fields as anomalies/perturbations relative to the reference data has reasonable performance through the control period, 2002-2012.

The NARR surface energy balance terms are plotted in Fig. 6. There are differences between the observed and NARR surface energy budgets (Figs. 6a-6d), with the highest relative errors in the turbulent fluxes. Sensible heat flux is systematically too low in the NARR reconstruction (Fig. 6c), while net radiation is too high (Fig. 6b). In addition, there is a small but systematic overestimation of the latent heat flux (Fig. 6d). Errors in Q^* and Q_H are each of order 10 W m^{-2}, and they compensate to give good estimates of Q_N and summer melt (Figs. 6e, 6f).

The two biases may be a result of differences in surface conditions in the model vs. the actual system. Net radiation is too high because albedo in the model is too low (Fig. 6a), particularly in the month of September. We do not adequately represent the effect of fresh snows that typically arrive in September and brighten the glacier surface. May and September are both mixed months on the glacier, with snowfall alternating with periods of melting. This raises the average albedo on the glacier, but our albedo parameterization does not capture this.

Similarly, we assume that the glacier surface is at the melting point throughout the melt season, May through September, but in truth it often drops below 0°C overnight and on cold days, particularly in the shoulder season once again. The assumption of a 0°C surface when the average surface temperature is less than this may explain the systematic underestimation of sensible heat flux (Fig. 6c) and overestimation of latent heat flux (Fig. 6d).

We discuss these biases further in Section 7. While it is only happenstance that the errors cancel out to give good estimates of Q_N and total summer melt, the interannual variability in Q_N, Q_H and Q_E is well-captured and points to some underlying skill in the NARR-based reconstructions.

Trends in most of the NARR energy fluxes are small or insignificant over the 36 years, relative to interannual variability. There is a positive trend in the net radiation (Fig. 6b), +0.3 W/m^2 yr^{-1}, or +11 W/m^2 over the 36-year period. Modelled albedo from the NARR energy balance and summer snow evolution has a small but statistically insignificant positive trend, so the increase in net radiation is only partially explained by this; it is primarily a result of increasing incident shortwave radiation, which must be due to decreasing cloud cover in the climate reanalysis.

In relative terms, latent heat flux has the most significant trend, +0.13 W/m^2 yr^{-1}, or +5 W/m^2 over the NARR period (Fig. 6d). This is consistent with the increase in humidity observed in Fig. 5. Net energy has a trend of +0.51 W/m^2 yr^{-1} (+18 W/m^2 over 36 years). This can mostly be attributed to the increases in net radiation and latent heat flux, although sensible heat flux also has a small positive trend over this period. The resultant trend in melt is +11 mm yr^{-1}, which represents 396 mm over 36 years: a 13% increase. The observational data is too brief to assess the presence or absence of trends, or to compare with those in the reanalysis.

The Cryosphere Discuss., doi:10.5194/tc-2016-6, 2016
Manuscript under review for journal The Cryosphere
Published: 29 January 2016

7. Discussion

The perturbation method for calculating surface energy balance and melt anomalies is a general approach that can be adopted to explore meteorological influences on melt in different glacier environments, or to model variations in time at a particular site. Application of the NARR reanalysis data at Haig Glacier is an example of the latter, and it could similarly be applied to future projections.

For Haig Glacier, which is a typical mid-latitude mountain glacier, summer melt is sensitive to most meteorological conditions. Based on the interannual variability in summer weather measured at our site from 2002-2012, fluctuations in cloud conditions (incoming shortwave radiation), albedo, and temperature have the strongest influence on summer melt, in that order. Changes in humidity can have a comparable effect to temperature, through its strong influence on incoming longwave radiation. Variations in wind are less influential at our site.

These results do not necessarily explain why glaciers are so sensitive to temperature change, as they clearly are in natural settings (e.g., Marzeion et al., 2014). Increase in temperature impact the glacier energy balance through both the sensible and incoming longwave fluxes, but the direct impacts on net energy and melt could easily be compensated by other systematic changes in the energy budget, such as decreases in shortwave radiation due to increased cloudiness.

There are two possible explanations here. One is that other systematic changes are not occurring in conjunction with the increase in temperature; variability in incoming shortwave radiation can be high, but it may not have a systematic trend like the well-documented increase in temperature in most regions. Where systematic, it may go in the opposite direction, as has been observed at Haig Glacier: warm summers at this site typically coincide with persistent ridging, subsidence, and clear-sky conditions, with positive anomalies in incoming shortwave radiation. It is difficult to say how general this result is, and whether it is typical of other regions.

The second and more general explanation involves indirect feedbacks of a temperature change. Snow/ice albedo is a sensitive variable in Table 3 and it is also a strong melt-season feedback, which is not captured in the isolated meteorological perturbations. A longer and more intense melt season gives rise to lower albedo through several influences: higher impurity and water content, an earlier transition from seasonal snow cover to glacial ice, and a greater area of the glacier that loses its seasonal snowpack (i.e., low accumulation area ratio). These positive feedbacks also operate (in reverse) under a cool perturbation. Albedo feedbacks can therefore amplify and exceed the initial temperature perturbation, as shown in Fig. 3, and may explain the high sensitivity of glaciers and ice sheets to perturbations in air temperature.

Other than albedo feedbacks, there are several other indirect impacts of a temperature change, including: (i) a longer melt season, starting earlier and ending later, (ii) a greater fraction of time spent above 0°C during the melt season, i.e., with reduced overnight cooling and refreezing, and (iii) an increase in the frequency of summer rain vs. snow events. Summer snow events have an important impact on surface albedo, with fresh snow strongly attenuating melt. Each of these processes contributes to the strong impact of increased temperatures on glacier melt.

Meteorological variables do not vary as idealistically as the simple experiments in this paper. In reality everything is varying at once, and different weather systems will have tendencies for the combined meteorological perturbations to compensate (buffer) or accentuate (amplify) impacts on energy balance and melt. An investigation of specific weather systems and their associated meteorological and energy balance conditions is recommended for followup work.

This is implicit in the NARR-driven energy balance and melt reconstructions, which represents a reconstruction of the actual daily weather and energy fluxes at the site from 1979-2014. Using the NARR fields as perturbations to the mean observed conditions at the site, net energy and melt are reasonably well simulated relative to the in situ data from 2002-2012. The results indicate positive trends in humidity, incoming surface-level shortwave radiation, net energy, and melt over the study period, along with a small positive trend in temperature. The reconstructed increase in melt over the 36 years is relatively modest, 13%, and is mostly related to increased net shortwave radiation and latent heat flux.

Biases in the NARR radiative fluxes are high. The perturbation approach removes the mean bias, but the interannual variability in these fluxes is not well-represented, undermining confidence in the NARR-based melt reconstructions for the glacier. It is not easy to assess whether the results are reasonable, since the period of direct observations is too short to assess trends. The glacier is in a state of emphatic retreat (Marshall, 2014), with a mean net balance of –910 mm water equivalent (w.e.) from 2002-2012; no years had a positive mass balance over this period.

Measurements prior to 2001 are lacking, so it is difficult to assess whether this negative balance is anomalous in the context of the last 36 years. Nearby Peyto glacier has a mass balance record running from 1966 to present. At Peyto, the mean net balance from 1979-2001 was –680 mm w.e. Mass loss increased at Peyto in the 2000s, with a mean net balance of −820 mm w.e. for 2002-2012 (WGMS, 2014) and a linear trend of −10.3 mm w.e. yr^{-1} through the full period. Seasonal mass balance data are available from Peyto Glacier for most years from 1966-1995 (Demuth and Keller, 2006), over which period the mean winter balances was 1195 mm w.e. If one makes the assumption that winter mass balance has not changed, this corresponds to a summer mass balance of −1875 mm w.e. from 1979-2001 and –2015 mm w.e. from 2002-2012, a 7.5% increase in melting. This is probably a poor assumption, and different scenarios can be examined, but the estimate of change in summer melt is similar to the NARR-derived value for Haig Glacier. This argues for a ~10% increase in melt over the last 36 years at these two sites.

The biases in our NARR-based energy balance point to model improvements that are possible, particularly with respect to our treatment of the glacier surface albedo and temperature. A better treatment of summer snowfall and late-summer snow accumulation is needed, as well as modelling of the surface temperature evolution through the melt season. These challenges are less of a problem in the core summer melt season, June through August, when surface temperatures remain close to 0°C and summer snowfall is less common, but these model improvements are needed in the shoulder season, May and September. A model of the glacier surface layer including conductive heat fluxes is required to properly address the surface temperature question, allowing a direct prediction of T_S. Such a model needs to consider meltwater percolation, refreezing, and remelting, as latent heat effects act to keep temperatures at the melting point through much of the melt season. This is beyond our current scope, but is recommended for followup studies.

The Cryosphere Discuss., doi:10.5194/tc-2016-6, 2016
Manuscript under review for journal The Cryosphere
Published: 29 January 2016

8. Conclusions

The goal of this work is to develop an energy balance model that can be driven by meteorological perturbations for glacier mass balance modelling. This allows a more complete treatment of the meteorological influences on melting than is possible with empirical melt models. Theoretical and numerical models exploring surface energy balance on Haig Glacier in the Canadian Rockies provide insight into melt sensitivity to different meteorological forcings. Our main findings are as follows:

1. Incoming shortwave radiation (cloud conditions) and albedo variations are the strongest controls on year-to-year variability in summer melt at our site.
2. Temperature and humidity also exert a significant impact on interannual melt variability, through the turbulent fluxes and incoming longwave radiation.
3. When feedbacks of a change in atmospheric temperature are included (e.g., a longer melt season, less summer snowfall, and reduced albedo), the temperature sensitivity is doubled and is comparable to the sensitivity to incoming shortwave radiation.
4. The results of theoretical perturbations are in agreement with the empirical perturbation for all variables except for the specific humidity (40 and 9 Wm^{-2} $(g/kg)^{-1}$ for the change in net energy from the theoretical and empirical sensitivity calculations, respectively). This difference may be a result of the strong sensitivity of our longwave radiation parameterization to changes in humidity in the theoretical results, which is not captured from the in situ data when we vary only one meteorological parameter at a time.

These results are based on perturbations of variables in isolation. To explore more realistic scenarios with multiple variables changing in concert, we use the perturbation approach to construct the past evolution of Haig Glacier energy balance based on NARR meteorological output from 1979 to 2014. All energy fluxes exhibit an increasing trend, producing a ca. 10% increase in summer melt extent over this period. Net radiation is the primary driver of this increase, driven by increases in incoming shortwave radiation and reduced albedo. Humidity and latent heat flux increases are also be important at this site in the NARR reconstructions, while summer temperature increases appear to play a tertiary role.

This contribution is an initial step, introducing the foundation for an energy balance sensitivity approach to quantify glacier sensitivity to meteorological variability and climate change. We examine this in detail at a site in the Canadian Rocky Mountains, with results that are specific to this site. However, this modelling approach for glacier energy and mass balance is well-suited to a distributed energy balance model, applying the perturbation approach to mountain-range scale. Climate models simulate all of the relevant meteorological fields, and both past reanalysis and future projections can be applied using the perturbation approach introduced here. Issues associated with model bias can be effectively avoided through this approach, as long as something is known of the baseline conditions at a site. Meteorological sensitivities under different climate regimes (e.g., maritime, polar, or tropical conditions) can also be explored using this framework, to help understand the differences in glacier sensitivity to climate change in different regions.

Acknowledgements

We thank the Natural Sciences and Engineering Research Council (NSERC) of Canada for longterm support of the Haig Glacier study. Samaneh Ebrahimi is financially supported in part through the Alberta Water Research Institute project Predicting Alberta's Water Future. We are indebted to numerous graduate students and research assistants who have helped to collect data and maintain instrumentation at Haig Glacier since 2001.

References

Andersen, M.L., Larsen, T.B., Nettles, M., Elosegui, P., van As D., Hamilton, G.S., Stearns, L.A., Davis, J.L., Ahlstrøm, A.P., de Juan, J., Ekström, G.L.: Spatial and temporal melt variability at Helheim Glacier, East Greenland, and its effect on ice dynamics. J, Geophys. Res.-Earth Surface (2003–2012)., 115, F4, doi:10.1029/2010JF001760, 2010.

Andreas, E. L.: Parameterizing scalar transfer over snow and ice: a review, J. Hydrometeorol., 3, 417-432, 2002.

Arnold, N. S., Willis, I. C., Sharp, M. J., Richards, K. S., and Lawson, M.J.: A distributed surface energy-balance model for a small valley glacier. I. Development and testing for Haut Glacier d'Arolla, Valais, Switzerland, J. Glaciol., 42, 77-89, 1996.

Braithwaite, R.J., Raper, S.C.: Glaciers and their contribution to sea level change. Physics and Chemistry of the Earth, Parts A/B/C., 27, 1445-54, 2002.

Braun, M. and Hock, R.: Spatially distributed surface energy balance and ablation modelling on the ice cap of King George Island (Antarctica), Global Planet. Change, 42, 45-58, 2004.

Brock, B. W., Willis, I. C., and Sharp, M. J.: Measurement and parameterisation of albedo variations at Haut Glacier d'Arolla, Switzerland, J. Glaciol., 46, 675-688, 2000.

Brutsaert, W.: On a derivable formula for long-wave radiation from clear skies, Water Resour. Res., 11, 742-744, 1975.

Clarke, G. K. C., Jarosch, A. H., Anslow, F. S., Radić V., and Menounos, B.: Projected deglaciation of western Canada in the twenty-first century, Nat. Geosci. 8, 372-377, 2015.

Cuffey, K. M., and Paterson, W. S. B.: The Physics of Glaciers, 4th Ed., Academic Press, Amsterdam, 2010.

The Cryosphere Discuss., doi:10.5194/tc-2016-6, 2016
Manuscript under review for journal The Cryosphere
Published: 29 January 2016

Demuth, M.N., and Keller, R.: An assessment of the mass balance of Peyto Glacier (1966-1995) and its relation to recent and past-century climatic variability, In: Peyto Glacier: One Century of Science, National Hydrology Research Institute Science Report Series #8, Demuth, M.N., Munro, D.S., and Young, G.J., Environment Canada, Saskatoon, Sask., 83-132, 2006.

Denby, B., Greuell, W., Oerlemans, J.: Simulating the Greenland atmospheric boundary layer. Tellus A. 1., 54, 512-28, 2002.

De Woul, M., Hock, R.: Static mass-balance sensitivity of Arctic glaciers and ice caps using a degree-day approach. Ann Glaciol., 42, 217-24, 2005.

Ebrahimi, S., and Marshall, S. J.: Parameterization of incoming longwave radiation at glacier sites in the Canadian Rocky Mountains, J. Geophys. Res.-Atmos., in press, doi: 10.1002/2015JD023324, 2015.

Favier, V., Wagnon, P., Chazarin, J. P., Maisincho L., and Coudrain, A..: One-year measurements of surface heat budget on the ablation zone of Antizana Glacier 15, Ecuadorian Andes, J. Geophys. Res.-Atmos. (1984-2012), 109, D18, doi: 10.1029/2003JD004359, 2004.

Giesen, R. H., Van den Broeke, M. R., Oerlemans, J., and Andreassen, L.M.: The surface energy balance in the ablation zone of Midtdalsbreen, a glacier in southern Norway: Interannual variability and the effect of clouds, J. Geophys. Res.-Atmos. (1984-2012), 113, D21, doi:10.1029/2008JD010390, 2008.

Greuell, W., and Smeets, P.: Variations with elevation in the surface energy balance of the Pasterze (Austria). J. Geophys. Res.-Atmos. (1984-2012), 106, D23, 31717-31727, 2001.

Hirose, J. M. R., and Marshall, S. J.: Glacier meltwater contributions and glacio-meteorological regime of the Illecillewaet River Basin, British Columbia, Canada, Atmos.-Ocean, 51, 416-435, doi:10.1080/07055900.2013.791614, 2013.

Hock, R.: Glacier melt: a review of processes and their modelling, Prog. Phys. Geog., 29, 362-391, 2005.

Hock, R. and Holmgren, B.: Some aspects of energy balance and ablation of Storglaciären, Sweden, Geografiska Annaler, 78A, 121-131, 1996.

Hock, R. and Holmgren, B.: A distributed surface energy-balance model for complex topography and its application to Storglaciären, Sweden, J. Glaciol., 51, 25-36, 2005.

Klok, E. J., and Oerlemans, J.: Model study of the spatial distribution of the energy and mass balance of Morteratschgletscher, Switzerland, J. Glaciol., 48, 505–518, 2002.

Lhomme, J. P., Vacher, J. J., and Rocheteau, A.: Estimating downward long-wave radiation on the Andean Altiplano, Agr. Forest Meteorol., 145, 139–148, 2007.

Marshall, S. J.: Meltwater runoff from Haig Glacier, Canadian Rocky Mountains, 2002–2013, Hydrol. Earth Syst. Sci., 18, 5181–5200, doi:10.5194/hess-18-5181-2014, 2014.

Marzeion, B., Cogley, J. G., Richter, K., and Parkes, D.: Attribution of global glacier mass loss to anthropogenic and natural causes, Science, 345, 919-921, 2014.

Mesinger, F., DiMego, G., Kalnay, E., Mitchell, K., Shafran, P.C., Ebisuzaki, W., Jovic, D., Woollen, J., Rogers, E., Berbery, E. H., and Ek, M. B.: North American Regional Reanalysis, Bull. Amer. Meteor. Soc., 87, 343-360, 2006.

Oerlemans, J.: Climate sensitivity of glaciers in southern Norway: application of an energy-balance model to Nigardsbreen, Hellstugubreen and Alfotbreen. J Glaciol., 38, 223-32, 1992.

Oerlemans, J., Fortuin, J.P.: Sensitivity of Glaciers and Small Ice Caps to Greenhouse Warming. Science., 258, 115-7, 1992.

Oerlemans, J., and Klok, E. J.: Energy balance of a glacier surface: analysis of AWS data from the Morteratschgletscher, Switzerland. Arct. Antarct. Alp. Res., 34, 115-123, 2002.

Oke, T.R.: Boundary Layer Climates, 2nd Ed, Psychology Press, New York, 435, 1987.

Radić, V., and Hock, R.: Regionally differentiated contribution of mountain glaciers and ice caps to future sea-level rise, Nat. Geosci., 4, 91-94, 2011.

Sedlar, J., and Hock, R.: Testing longwave radiation parameterizations under clear and over-cast skies at Storglaciaren, Sweden, The Cryosphere, 3, 75–84, doi:10.5194/tc-3-75-2009, 2009.

Wagnon P. W., Ribstein, P., Francou, B., and Pouyaud, B.: Annual cycle of energy balance of Zongo Glacier, Cordillera Real, Bolivia, J. Geophys. Res., 104, 3907-3923, 1999.

Wagnon P. W., Sicart, J. E., Berthier, E., and Chazarin, J. P.: Wintertime high-altitude surface energy balance of a Bolivian glacier, Illimani, 6340 m above sea level, J. Geophys. Res., 108 (D6 4177), doi:10.1029/2002JD002088, 2003.

Willis, I. C., Arnold, N. S., and Brock, B. W.: Effect of snowpack removal on energy balance, melt and runoff in a small supraglacial catchment, Hydrol. Process., 16, 2721-2749, 2002.

WGMS: World Glacier Monitoring Service, Zurich, Switzerland. Glacier Mass Balance Bulletins (M. Zemp et al., Eds.), ICSU(WDS)/IUGG(IACS)/UNEP/UNESCO/WMO, data available at http://wgms.ch/gmbb.html, 2014.

The Cryosphere Discuss., doi:10.5194/tc-2016-6, 2016
Manuscript under review for journal The Cryosphere
Published: 29 January 2016

Table 1. Mean monthly weather conditions at Haig Glacier, Canadian Rocky Mountains, 2002-2012 during the summer melt season ± one standard deviation, based on automatic weather station measurements at an elevation of 2660 m, in the upper ablation zone of the glacier.

Month	T (°C)	h (%)	e_v (mb)	q_v (g/kg)	P (mb)	v (m/s)
May	−1.4 ± 1.1	73 ± 4	4.0 ± 0.4	3.4 ± 0.4	743.0 ± 2.4	2.8 ± 0.2
June	2.6 ± 0.9	73 ± 6	5.5 ± 0.5	4.6 ± 0.4	748.1 ± 1.4	2.6 ± 0.2
July	6.9 ± 1.4	62 ± 5	6.4 ± 0.4	5.3 ± 0.3	751.2 ± 1.6	2.8 ± 0.3
August	5.9 ± 1.1	64 ± 7	6.1 ± 0.4	5.1 ± 0.4	750.8 ± 1.4	2.5 ± 0.2
Sept	2.1 ± 1.8	71 ± 10	5.0 ± 0.4	4.2 ± 0.3	748.4 ± 1.8	3.0 ± 0.4
JJA	5.1 ± 0.8	67 ± 4	5.7 ± 0.4	4.8 ± 0.3	750.0 ± 1.1	2.6 ± 0.2
MJJAS	3.2 ± 0.7	69 ± 4	5.3 ± 0.3	4.3 ± 0.3	748.3 ± 1.4	2.7 ± 0.2

The Cryosphere Discuss., doi:10.5194/tc-2016-6, 2016
Manuscript under review for journal The Cryosphere
Published: 29 January 2016

Table 2. Mean monthly surface energy balance at Haig Glacier, Canadian Rocky Mountains, 2002-2012 during the summer melt season ± one standard deviation, based on automatic weather station measurements at an elevation of 2660 m, in the upper ablation zone of the glacier. All fluxes are in W m^{-2} and melt totals are in mm w.e.

Month	$Q_S{\downarrow}$	α_s	$Q_L{\downarrow}$	$Q_L{\uparrow}$	Q_H	Q_E	Q_N	*melt*
May	249 ± 24	0.76 ± 0.04	262 ± 11	298 ± 7	−1 ± 6	−16 ± 3	10 ± 20	230 ± 90
June	237 ± 23	0.70 ± 0.05	281 ± 12	306 ± 3	14 ± 4	−5 ± 4	58 ± 19	510 ± 130
July	239 ± 19	0.57 ± 0.06	280 ± 7	311 ± 1	36 ± 9	3 ± 5	114 ± 28	930 ± 210
August	203 ± 29	0.38 ± 0.07	278 ± 11	310 ± 1	28 ± 6	−1 ± 4	126 ± 22	1050 ± 175
Sept	140 ± 30	0.59 ± 0.09	274 ± 11	305 ± 4	16 ± 11	−10 ± 5	34 ± 22	360 ± 170
JJA	227 ± 14	0.55 ± 0.06	280 ± 6	309 ± 1	27 ± 4	−3 ± 4	99 ± 20	2490 ± 460
MJJAS	215 ± 17	0.60 ± 0.04	276 ± 7	305 ± 2	22 ± 5	−6 ± 3	72 ± 17	3080 ± 620

The Cryosphere Discuss., doi:10.5194/tc-2016-6, 2016
Manuscript under review for journal The Cryosphere
Published: 29 January 2016

The Cryosphere Discussions

Table 3. Surface energy balance sensitivity to meteorological perturbations over a melting glacier surface, from direct feedbacks only. All energy flux perturbations are expressed in W m^{-2}, and the melt perturbation, δm, is calculated assuming that δQ_N holds for JJA (92 days).

Perturbation	$\delta Q_S^{\downarrow}$	$\delta\alpha$	δQ_S^{net}	$\delta Q_L^{\downarrow}$	δQ_H	δQ_E	δQ_N	δm (mm)
δT = 1°C, δh = 0	0	0	0	4.5	4.2	3.5	12.2	288
δT = 1°C, δq_v = 0, $\delta\tau$ = 0	0	0	0	–4.5	4.2	0	–0.2	–6
δT = 1°C, δq_v = 0, $\delta\tau$ = 0.03	15.0	0	6.8	–4.5	4.2	0	6.5	155
δq_v = 1 g kg^{-1}, $\delta\tau$ = 0	0	0	0	29.3	0	10.5	39.7	943
δq_v = 1 g kg^{-1}, $\delta\tau$ = –0.12	–41.8	0	–18.8	29.3	0	10.5	20.9	497
δv = 1 m s^{-1}	0	0	0	0	8.3	–1.4	6.9	164
δQ_S = 1 W m^{-2}	0.6	0	0.3	0	0	0	0.3	7
$\delta\tau$ = 0.05	18.0	0	8.1	0	0	0	8.1	192
$\delta\alpha_S$ = 0.1	0	0.1	–22.7	0	0	0	–22.7	–539
1σ, all (JJA)	14.0	–0.06	20.8	0.3	5.6	7.5	34.0	808
1σ, all (MJJAS)	17.0	–0.04	16.0	5.5	4.6	7.3	33.5	1323

The Cryosphere Discuss., doi:10.5194/tc-2016-6, 2016
Manuscript under review for journal The Cryosphere
Published: 29 January 2016

Table 4. Net energy balance sensitivity to meteorological perturbations in the surface energy balance model, based on regressions to the sensitivity curves in Fig. 2. Also shown is the change in net energy associated with a 1-σ increase in each parameter, averaged over MJJAS.

Perturbation	*Sensitivity*	δQ_N for $+1\sigma$
$\delta T = \pm 2°C$, $\delta q_v = 0$	$\partial Q_N/\partial T = 8.6$ W m^{-2} (°C)$^{-1}$	+6.0 W m^{-2}
$\delta q_v = \pm 50\%$, $\delta\tau = 0$	$\partial Q_N/\partial q_v = 8.7$ W m^{-2} (g/kg)$^{-1}$	+2.6 W m^{-2}
$\delta v = \pm 50\%$	$\partial Q_N/\partial v = 4.8$ W m^{-2} (m/s)$^{-1}$	+1.0 W m^{-2}
$\delta Q_S^{\downarrow} = \pm 10$ W m^{-2}	$\partial Q_N/\partial Q_S^{\downarrow} = 0.67$ W m^{-2} (W m^{-2})$^{-1}$	+11.1 W m^{-2}
$\delta\alpha_S = 0.1$	$\partial Q_N/\partial\alpha_S = -14.1$ W m^{-2} (0.1)$^{-1}$	−5.6 W m^{-2}

Table 5. Mean NARR fields for the Haig Glacier grid cell, MJJAS, 2002-2012. Also shown are linear correlations for the mean daily values of each field from May-September.

	T (°C)	h (%)	e_v (mb)	q_v (g/kg)	v (m/s)	P (mb)	$Q_S^{\downarrow}$ (W m^{-2})	$Q_L^{\downarrow}$ (W m^{-2})
Haig AWS	3.2	69	5.3	4.3	2.7	748.3	215	276
NARR	7.1	67	7.4	5.9	3.4	783.9	291	265
bias	3.9	−2	2.1	1.6	0.7	35.6	76	−11
correlation	0.98	0.81	0.96	0.96	0.60	0.92	0.88	0.69

The Cryosphere Discuss., doi:10.5194/tc-2016-6, 2016
Manuscript under review for journal The Cryosphere
Published: 29 January 2016

Table 6. NARR vs. in situ observations of mean monthly surface energy balance and melt conditions, 2002-2012. The table shows the raw NARR predictions and the NARR results using the perturbation method. Values can be compared with the *in situ* data in Table 2.

NARR raw data							
Month	$Q_S^{\downarrow}$	α_s	$Q_L^{\downarrow}$	Q_H	Q_E	Q_N	*melt*
May	301 ± 14	0.74 ± 0.02	251 ± 7	14 ± 8	−10 ± 6	24 ± 18	320 ± 110
Jun	322 ± 13	0.55 ± 0.08	273 ± 7	45 ± 7	15 ± 7	170 ± 38	1300 ± 300
Jul	335 ± 11	0.26 ± 0.02	276 ± 5	67 ± 11	35 ± 9	317 ± 29	2540 ± 230
Aug	287 ± 10	0.25 ± 0.00	270 ± 7	58 ± 9	26 ± 5	260 ± 17	2090 ± 140
Sep	209 ± 10	0.26 ± 0.01	254 ± 5	36 ± 10	5 ± 4	139 ± 18	1100 ± 130
JJA	315 ± 6	0.35 ± 0.03	273 ± 3	57 ± 7	25 ± 5	249 ± 20	5925 ± 486
MJJAS	291 ± 6	0.41 ± 0.02	265 ± 3	44 ± 6	14 ± 3	182 ± 14	7340 ± 520
NARR perturbed data							
Month	$Q_S^{\downarrow}$	α_s	$Q_L^{\downarrow}$	Q_H	Q_E	Q_N	*melt*
May	249 ± 12	0.79 ± 0.01	258 ± 7	−6 ± 5	−20 ± 4	−16 ± 12	95 ± 55
Jun	242 ± 10	0.72 ± 0.02	278 ± 7	12 ± 4	−8 ± 4	44 ± 17	370 ± 110
Jul	240 ± 8	0.55 ± 0.07	280 ± 5	33 ± 8	−3 ± 5	117 ± 36	940 ± 280
Aug	206 ± 7	0.31 ± 0.07	276 ± 7	26 ± 6	−4 ± 3	138 ± 18	1110 ± 150
Sep	135 ± 7	0.27 ± 0.01	268 ± 5	9 ± 7	−13 ± 3	67 ± 12	540 ± 90
JJA	229 ± 4	0.51 ± 0.05	278 ± 3	24 ± 5	−5 ± 3	100 ± 20	2410 ± 450
MJJAS	218 ± 5	0.52 ± 0.03	276 ± 3	15 ± 4	−9 ± 2	71 ± 12	3060 ± 450

The Cryosphere Discuss., doi:10.5194/tc-2016-6, 2016
Manuscript under review for journal The Cryosphere
Published: 29 January 2016

The Cryosphere Discussions

Figures

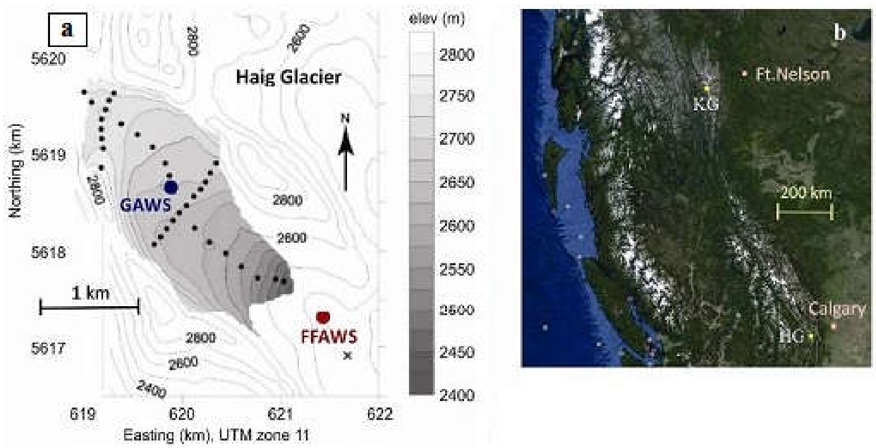

Figure 1. (a) The topography and automatic weather stations on Haig Glacier (denoted as GAWS in blue) and in the forefield (denoted as FFAWS in red), the smaller black dots are mass balance survey points. (b) The location of Haig Glacier is labelled HG,on the Google Earth map of Western Canada.

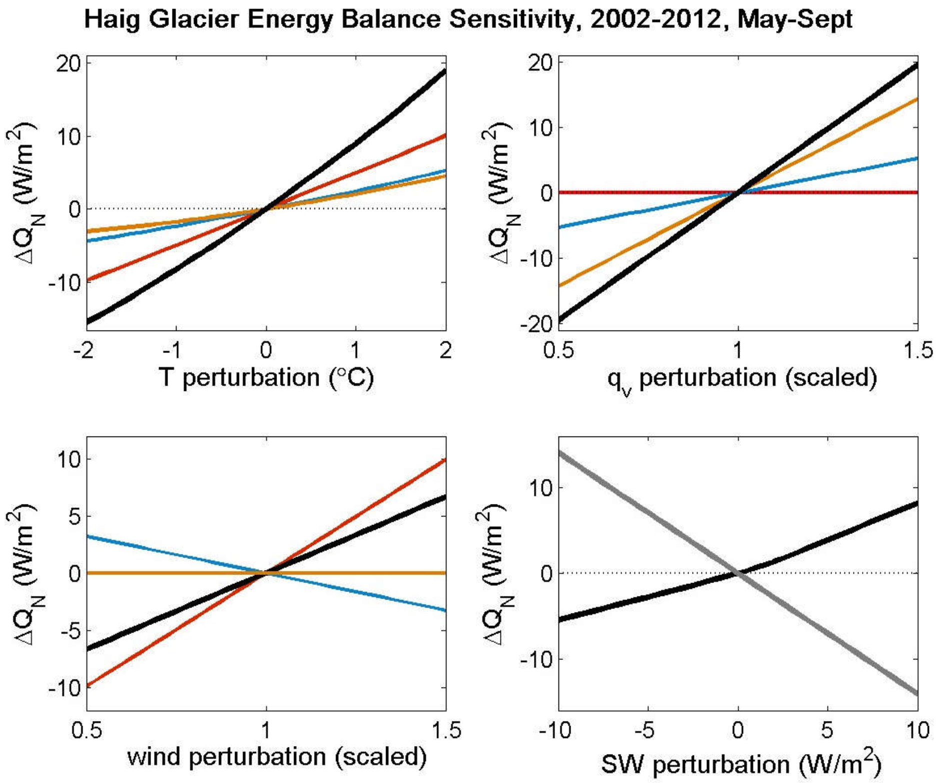

Figure 2. Sensitivity of the surface energy balance at Haig Glacier to a changes in (a) temperature, (b) specific humidity, (c) wind speed, and (d) shortwave radiation (black) and albedo (grey). Albedo perturbations are from –0.1 to 0.1 but are plotted as percent (–10 to +10%). For all plots, the black lines indicate the net radiation, red lines are the sensible heat flux, blue lines are the latent heat flux, and orange lines are the incoming longwave radiation. All lines are anomalies relative to the baseline data from the period 2002-2012, and indicate the mean sensitivity of the different energy fluxes over this period.

The Cryosphere Discuss., doi:10.5194/tc-2016-6, 2016
Manuscript under review for journal The Cryosphere
Published: 29 January 2016

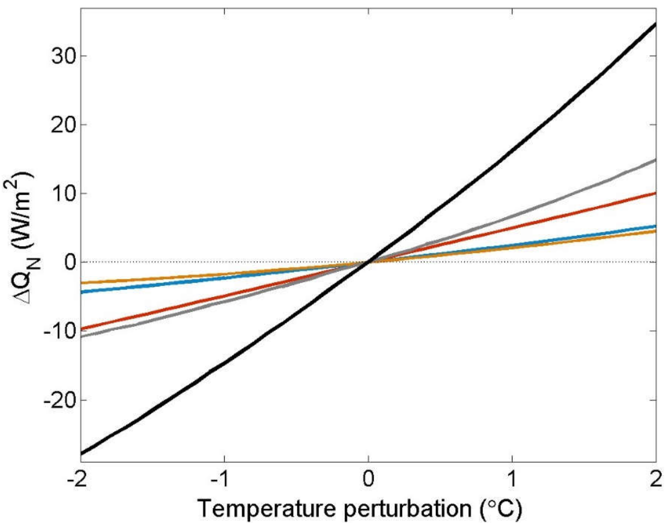

Figure 3. Modelled temperature sensitivity as in Fig. 2a, except with albedo feedbacks through the summer melt season. Black line: net energy. Grey line: net shortwave energy. Red line: sensible heat flux. Blue line: latent heat flux. Orange line: incoming longwave radiation.

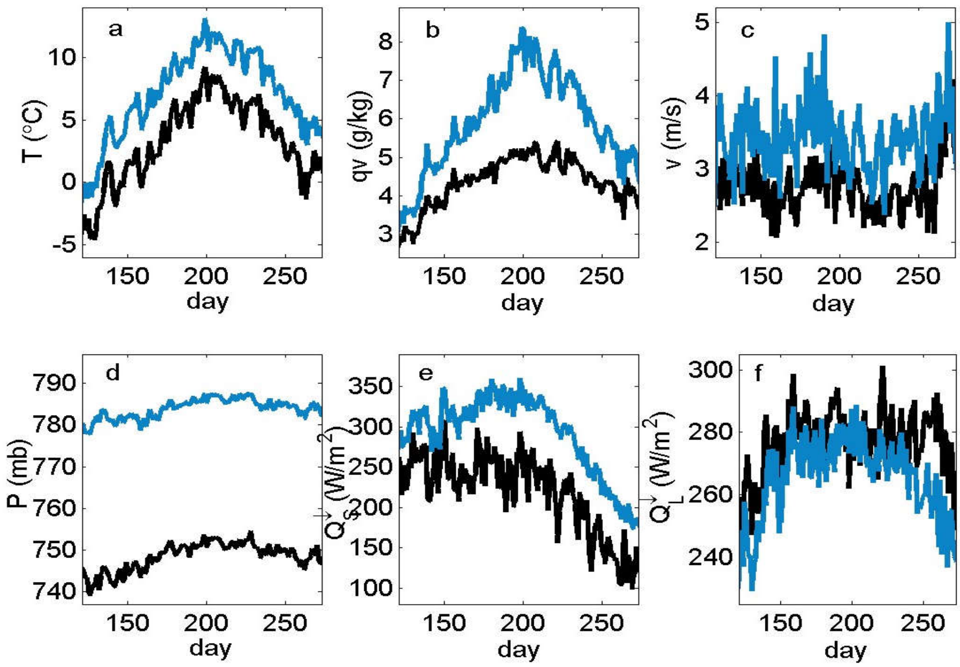

Figure 4. Daily evolution of NARR weather conditions (blue) vs. Haig Glacier AWS in situ data (black) through the melt season, May 1-Sept 30. Plots show the mean daily values from 2002-2012, for: (a) temperature, (b) specific humidity, (c) wind speed, (d) air pressure, (e) incoming shortwave radiation, and (f) incoming longwave radiation. Table 5 gives correlations.

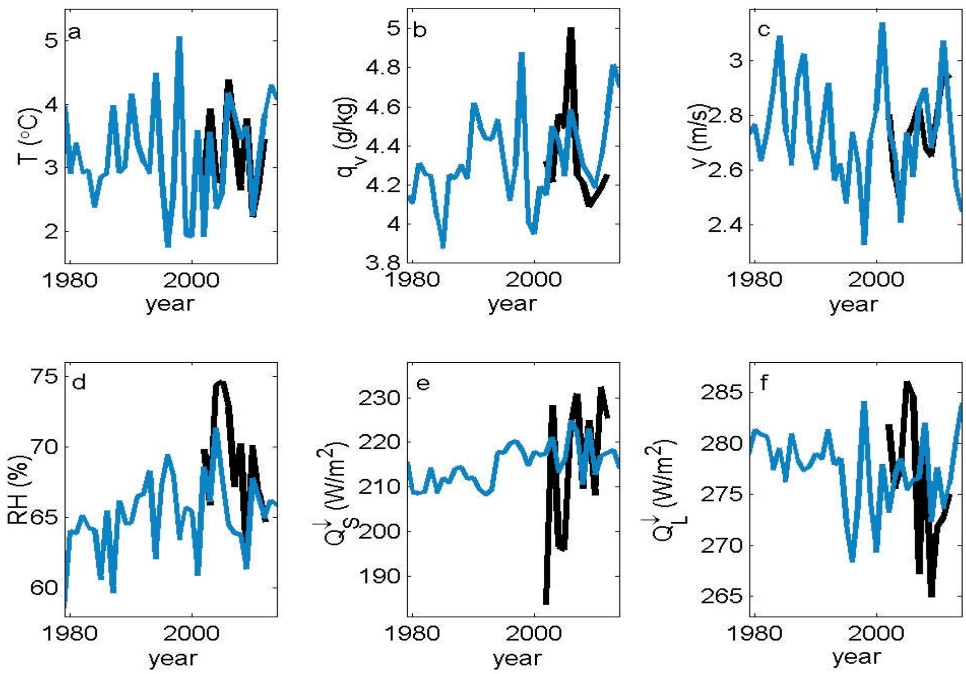

Figure 5. Mean melt season (MJJAS) weather conditions from the bias-corrected NARR output (blue), 1979-2014, and for the in situ data (black), 2002-2012: (a) temperature, (b) specific humidity, (c) wind speed, (d) relative humidity, (e) incoming shortwave radiation, and (f) incoming longwave radiation.

The Cryosphere Discuss., doi:10.5194/tc-2016-6, 2016
Manuscript under review for journal The Cryosphere
Published: 29 January 2016

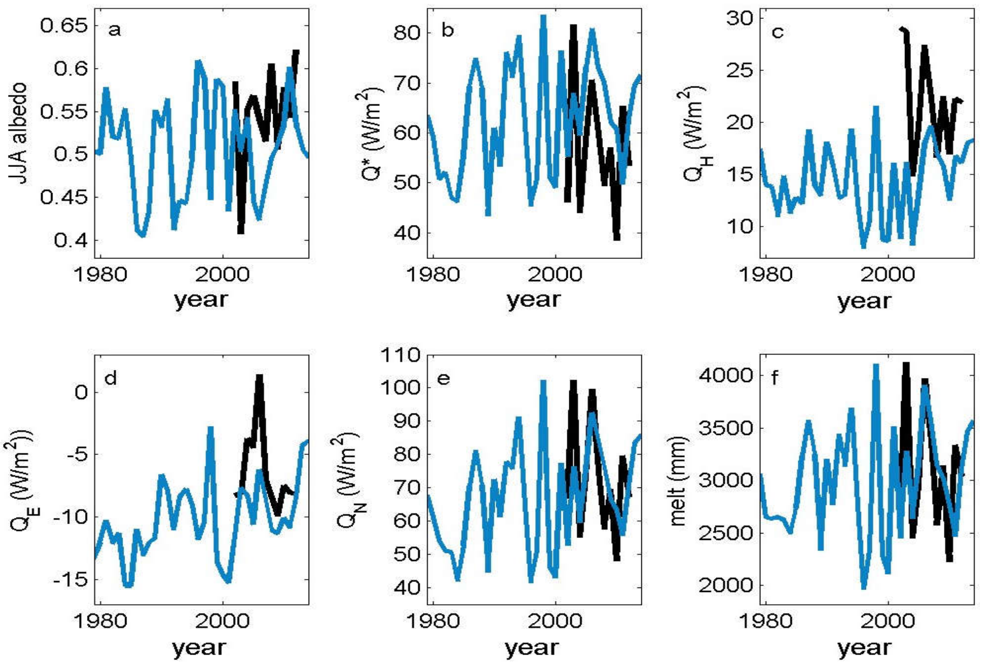

Figure 6. The evolution of modelled summer surface energy balance and melt from the perturbed NARR output (blue), 1979-2014, and from the in situ data (black), 2002-2012. (a) albedo, (b) net radiation, (c) sensible heat flux, (d) latent heat flux, (e) net energy, and (f) total summer melt (mm). All fields are for MJJAS except for albedo, which is shown for JJA, the main melt season.